Editors' Suggestion

Record-High T_c and Dome-Shaped Superconductivity in a Medium-Entropy Alloy TaNbHfZr under Pressure up to 160 GPa

Liyunxiao Wu,[1,2,*] Jianguo Si,[1,3,*] Shixue Guan,[4,*] He Zhang,[1,2] Jie Dou,[1,2] Jun Luo,[1] Jie Yang,[1] Hui Yu,[1,2] Jiawei Zhang,[1] Xiaoli Ma,[1] Pengtao Yang,[1,2] Rui Zhou,[1,3] Miao Liu,[1,3,5,†] Fang Hong,[1,2,3,‡] and Xiaohui Yu[1,2,3,§]

[1]*Beijing National Laboratory for Condensed Matter Physics and Institute of Physics, Chinese Academy of Sciences, Beijing 100190, China*

[2]*School of Physical Sciences, University of Chinese Academy of Sciences, Beijing 100190, China*

[3]*Songshan Lake Materials Laboratory, Dongguan, Guangdong 523808, China*

[4]*School of Applied Science, Beijing Information Science and Technology University, Beijing 100192, China*

[5]*Center of Materials Science and Optoelectronics Engineering, University of Chinese Academy of Sciences, Beijing 100049, China*

(Received 3 January 2024; revised 6 March 2024; accepted 25 March 2024; published 16 April 2024)

Superconductivity has been one of the focal points in medium and high-entropy alloys (MEAs-HEAs) since the discovery of the body-centered cubic (bcc) HEA superconductor in 2014. Until now, the superconducting transition temperature (T_c) of most MEA and HEA superconductors has not exceeded 10 K. Here, we report a TaNbHfZr bulk MEA superconductor crystallized in the BCC structure with a T_c of 15.3 K which set a new record. During compression, T_c follows a dome-shaped curve. It reaches a broad maximum of roughly 15 K at around 70 GPa before decreasing to 9.3 K at 157.2 GPa. First-principles calculations attribute the dome-shaped curve to two competing effects, that is, the enhancement of the logarithmically averaged characteristic phonon frequency $\omega_{\log}$ and the simultaneous suppression of the electron-phonon coupling constant λ. Thus, TaNbHfZr MEA may have a promising future for studying the underlying quantum physics, as well as developing new applications under extreme conditions.

DOI: 10.1103/PhysRevLett.132.166002

Superconductivity is a fascinating macroscopic quantum phenomenon. The cooperation or competition of superconductivity and other order parameters (charge density wave [1,2], spin density wave [3,4], pair density wave [5], etc.) has given complex phase diagrams for superconductivity. Dome-shaped superconductivity is one of the observations, which exists in various superconducting systems, such as kagome lattices [6,7], heavy fermions [8], copper oxide [9,10], and iron-based superconductors [11]. Interestingly, superconductivity can also be observed in amorphous materials, as well as dome-shaped superconductivity [12]. More recently, medium or high-entropy alloys (MEAs-HEAs) [13–22] have become a new platform to study superconductivity because of the expansion of the compositional space by multicomponent and the unpredictable properties indicated by the cocktail effect [23] that differs from single elements. This kind of alloy is distinguished by the presence of a well-defined crystal lattice in high symmetry, amorphous-type chemical (substitutional) disorders, and even numerous distortions. As a result, studying their intrinsic superconductivity contributes to a better understanding of the differences and physical mechanisms of superconductivity between crystallized and amorphous superconductors.

The definition of MEAs and HEAs depends on ΔS_{mix} (MEAs have a ΔS_{mix} between R and $1.5R$ [24,25], and HEAs have a ΔS_{mix} larger than $1.5R$ [13,26], where the R is the gas constant). Since the body-centered cubic (bcc) HEA superconductor was first reported in 2014 [27], the superconductivity in MEAs-HEAs has aroused broad interest. MEA-HEA superconductors are often synthesized using the electric arc melting method. There are also reports of producing thin films to enhance their potential applications [28–30], such as superconducting electronic circuits or device fabrication. Detailed theoretical studies of the electronic structures are also reported [31,32]. Until now, the crystal structures of MEA-HEA superconductors have primarily consisted of bcc, α—Mn, CsCl, and hexagonal-close-packed (hcp) structures [33–37]. In order to study the underlying physical mechanism, a common research method is chemical doping, which can manipulate the composition ratios between the principal elements of MEA-HEA superconductors. In the bcc phase [33,34], von Rohr *et al.* used arc melting of the elements under argon to synthesize $(\mathrm{TaNb})_{1-x}(\mathrm{HfZrTi})_x$, and they found a dome-shaped curve of dope-dependent T_c with the highest T_c (8.0 K) occurring in $x = 0.3$. At the same time, in α—Mn phase, Stolze *et al.* have studied superconductivity in $(\mathrm{ZrNb})_{1-x}(\mathrm{MoReRu})_x$, $(\mathrm{HfTaWIr})_{1-x}(\mathrm{Re})_x$ and $(\mathrm{HfTaWPt})_{1-x}(\mathrm{Re})_x$, and they found a nearly linear dependence of T_c on doping [35]. In contrast, in CsCl—phase, K. Stolze *et al.* discovered the opposite linear doping dependency of T_c compared to the α—Mn phase [36]. Different doping dependencies of T_c across various

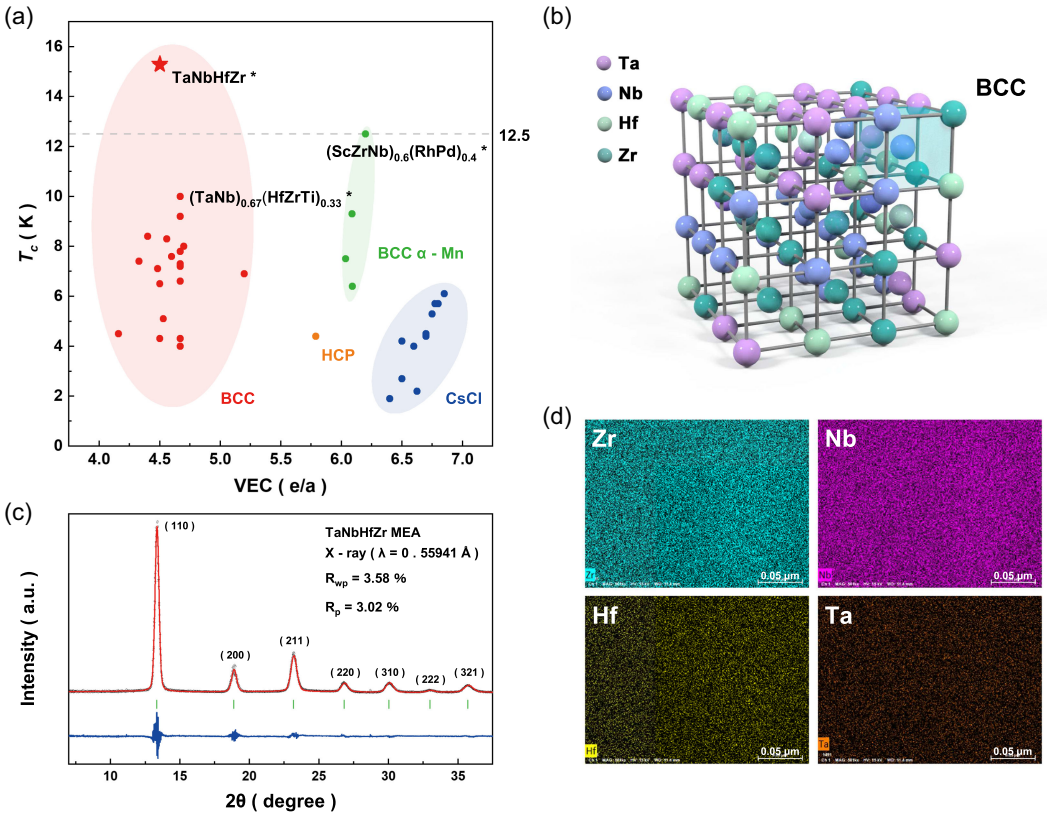

FIG. 1. (a) Valence electron count (VEC) dependence of the superconducting transition temperature (T_c) for some MEAs and HEAs including TaNbHfZr MEA. The data were taken from Refs. [27,33,35–37,39]. (The α—Mn phase derives from the low-temperature allotrope of manganese and is bcc with a relatively large crystallographic cell that contains more atoms than the simple bcc and CsCl-type structures in MEA and HEA superconductors) (* refers to high-pressure experiment) (b) Crystal structure of TaNbHfZr MEA. (c) XRD patterns of TaNbHfZr at ambient pressure. (d) EDX elemental mappings of TaNbHfZr.

structures demonstrate the complexity of the underlying physical mechanisms in MEA-HEA superconductors.

Compared to doping, pressure, as a relatively clean physical factor, is also frequently used to study superconductivity. The robustness of superconductivity is the most significant characteristic of MEA-HEA superconductors [24,38]. In 2017, researchers announced a HEA $(TaNb)_{0.67}(HfZrTi)_{0.33}$, which maintained structural integrity and zero electrical resistance under pressures up to 190.6 GPa [38]. T_c rises slowly with pressure, from around 7.7 K at ambient pressure to 10 K at roughly 60 GPa. As pressure is increased further, T_c essentially stays constant up to around 190 GPa. Superconductor $(ScZrNbTa)_{0.6}(RhPd)_{0.4}$ was also observed to exhibit a similar phenomenon under pressure [24]. T_c increases to 12.5 K upon compression but saturates at pressures of 30 GPa. The high ΔS_{mix} decreases the Gibbs' free energy, and hence phase stability is expected. So the discovery of the robustness of superconductivity under extremely high pressure was thought to be related to the high ΔS_{mix}. Given the variety of superconducting alloy types and the complex physical mechanisms reflected in doping research, the pressure dependence of superconducting transition temperature in MEA-HEA superconductors may exhibit different behaviors with those by changing the compositions, which is beneficial for the understanding of intrinsic behavior of the superconductivity.

The selection of experimental materials is based on two experimental facts. First, one of the most commonly utilized elements in the design of MEA and HEA with a reasonably high T_c is the Nb element [24]. Second, doping experiments demonstrate that MEA and HEA have the maximum T_c when the valence electron number is around 4.6 e/a [33,34]. So we choose quaternary TaNbHfZr MEA with a valence electron count of 4.5 e/a and present the crystal structure and physical properties at extreme pressures. The results show a dome-shaped superconductivity of up to 157.2 GPa with the highest T_c of 15.3 K at 71.6 GPa. First-principles calculations attribute the dome-shaped curve to two competing effects, that is, the enhancement of the logarithmically averaged characteristic phonon frequency $\omega_{\log}$ and the simultaneous suppression of the electron-phonon coupling constant λ. In fact, TaNbHfZr MEA's T_c is the highest value ever placed in MEAs and HEAs, which will be helpful for understanding the underlying quantum physics in the future. [Various MEA and HEA T_c are listed in Fig. 1(a)].

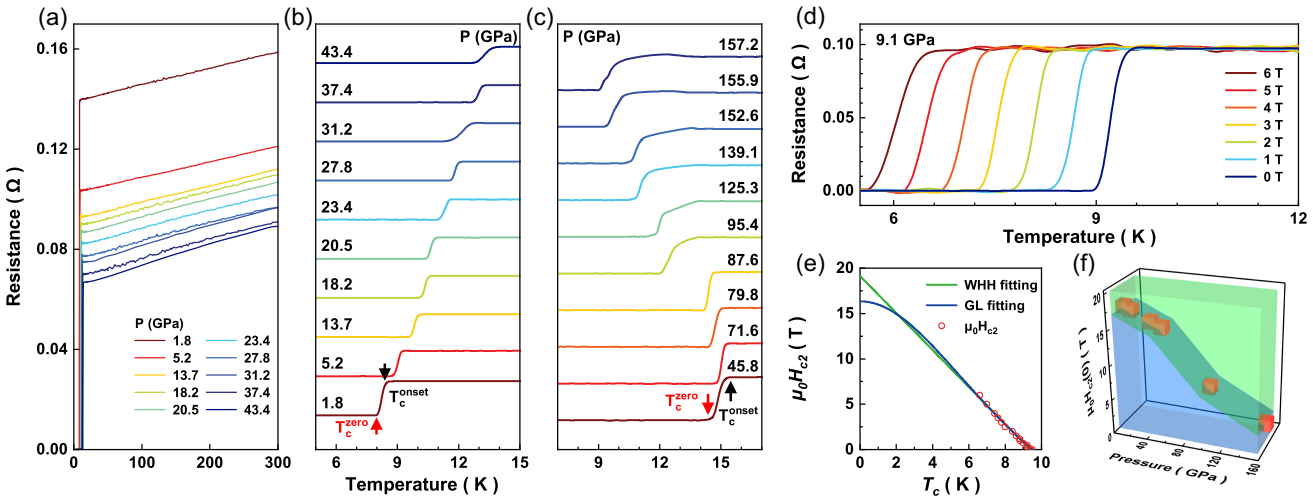

FIG. 2. Characterization of the superconductivity of the TaNbHfZr MEA at high pressure. (a) Temperature-dependent resistance of TaNbHfZr MEA from 1.8 to 43.4 GPa. (b) The enlarged view of the temperature-dependent resistance from 1.8 GPa to 43.4 GPa. (Except for data at 1.8 GPa, all other curves in b have been vertically shifted for clarity). The onset T_c^{onset} was determined as the temperature where resistivity starts to deviate from the extrapolated normal-state behavior. The T_c^{zero} was determined as the zero-resistivity temperature. (c) Temperature-dependent resistance of TaNbHfZr MEA from 45.8 to 157.2 GPa (enlarged view). (Except for data at 45.8 GPa, all other curves in c have been vertically shifted for clarity) (d) The resistive transition under different magnetic fields at 9.1 GPa. (e) The temperature dependence of the upper critical field $\mu_0 H_{c2}$ with the WHH model fitting and the Ginzburg-Landau function fitting. (f) The pressure dependence of the upper critical field at zero temperature $\mu_0 H_{c2}(0)$ fitted by the Ginzburg-Landau function.

X-ray diffraction (XRD) analysis at ambient pressure shows that the TaNbHfZr MEA crystallizes in a bcc structure [Fig. 1(b)], and the lattice parameter is $a = 3.4157$ Å [Fig. 1(c)]. The high-intensity peak with Miller index (110) can be seen clearly in Fig. 1(c). Figure 1(d) shows energy-dispersive x-ray spectroscopy (EDX) elemental mappings of TaNbHfZr, suggesting a homogeneous elemental distribution.

The T_c of TaNbHfZr at ambient pressure is 8.1 K (shown in the Supplemental Material Fig. S3 [40]). We performed high-pressure resistance measurements at different pressures. Temperature-dependent resistivity of TaNbHfZr from 1.8 to 31.2 GPa (2–300 K) is demonstrated in Fig. 2(a). At cryogenic temperatures [the enlarged view of the temperature-dependent resistance is shown in Fig. 2(b)], the TaNbHfZr MEA is revealed to be a superconductor. T_c linearly shifts from 8.5 K at 1.8 GPa to 14.0 K at 43.4 GPa. Here, we define T_c to be the onset temperature of the superconductivity T_c^{onset}. It is noteworthy that at pressures below 27.8 GPa, the temperature dependence curves of electrical resistance exhibit a linear relationship, which is different from the conventional behavior seen in Fermi liquid metals. Such behavior suggests the existence of possible electron correlations. However, no signature of spin or charge fluctuations are observed from ^{93}Nb-NMR measurements (shown in Supplement Material Fig. S4 [40]). Therefore, the T-linear electrical resistivity behavior may be attributed to the complexity associated with sample preparation and the pressurization process. At $T > T_c$, the normal state resistivity increases slowly with the temperature at all pressures, indicating poor metallic behavior. The very low residual resistivity ratio (RRR), which is found to be $\rho(300)/\rho(10) = 1.1$, points to the possibility of atomic-scale disorder in the MEA. Strain sensitivity is one of the most important metrics for strain materials, indicating their ability to change resistance under elastic deformation or pressure. We have determined the resistivity isotherms at various pressures in order to estimate this feature. At 300 K, the pressure coefficient of the resistance is -1.0×10^{-2} GPa^{-1}. It is worth noting that, under the same conditions, the widely used strain gauge alloy manganin exhibits analogous resistance changes by absolute value but with the reverse sign (resistivity increases with increasing pressure) [56,57]. Because of its significant tensoresistive effect, thermal stability, and superior mechanical properties, TaNbHfZr MEA is a potential metallic material for the development of sensitive components for tensometric transducers operating in extreme conditions.

Resistance measurements were also made over the extensive pressure range of 45.8–157.2 GPa in order to examine the superconducting behavior at higher pressures. Figure 2(c) shows the enlarged view of the temperature-dependent resistance. The results prove that the TaNbHfZr MEA exhibits superconductivity even at pressures as high as 157.2 GPa. T_c first reaches a broad maximum (around 15 K) within the pressure range of 45.8–79.8 GPa compared to lower pressure, which then drops to 9.3 K at 157.2 GPa. The maximum T_c in the experiment is 15.3 K at 71.6 GPa. In terms of all HEAs and MEAs currently known, 15.3 K set a new record to the best of our knowledge.

We conducted $R(T)$ measurements under various external magnetic fields at 9.1 GPa to confirm the presence of superconductivity in TaNbHfZr MEA. As can be seen in Fig. 2(d), the resistance transition gradually shifts to lower temperatures and becomes broader when magnetic fields are applied, which is a hallmark of the superconducting transition. Given that T_c is 6.6 K under 6 T, it is clear that the magnetic field has a significant impact on the transition. Using the same criteria as for zero-field resistivity measurements, we were able to determine the temperature variation of the upper critical field ($\mu_0 H_{c2}$) for the TaNbHfZr MEA, which is shown in Fig. 2(e). The resulting slope ($\mathrm{d}\mu_0 H_{c2}/\mathrm{d}T$) is -2.04057 T/K for the TaNbHfZr MEA. The data was fitted using the Werthamer-Helfand-Hohenberg (WHH) formula: $\mu_0 H_{c2}(0) = -0.693 T_c (\mathrm{d}\mu_0 H_{c2}/\mathrm{d}T)|_{T=T_c}$. Using $T_c =$ 9.5 K, the dirty limit $\mu_0 H_{c2}(0)^{\mathrm{WHH}}$ value was calculated to be 13.4 T [green line in Fig. 2(e)].

The data were also fitted with the Ginzburg-Landan (GL) formula: $\mu_0 H_{c2}(T) = \mu_0 H_{c2}(0) \times \{[1-(T/T_c)^2]/[1+(T/T_c)^2]\}$. In the full temperature range, the GL model provides a satisfactory fit to the experimental data. The calculated value of $\mu_0 H_{c2}(0)^{\mathrm{GL}}$ is 16.3 T. According to BCS theory, the Pauli limiting field for a superconductor can be described by $\mu_0 H_p = 1.84\ \mathrm{TK}^{-1} \times T_c$, that is, 17.5 T for the TaNbHfZr MEA sample, which is larger than the upper critical field at zero temperature $\mu_0 H_{c2}(0)$ [blue line in Fig. 2(e)]. TaNbHfZr's GL coherence length [$\xi_{\mathrm{GL}}(0)$] is calculated as 44.9 Å by the relation: $\xi^2_{\mathrm{GL}}(0) = [\phi_0/2\pi H_{c2}(0)]$, where $\phi_0 = h/2e$. It implies that the TaNbHfZr MEA contains significant electron-electron interaction.

To quantify the effect of the pressure on $\mu_0 H_{c2}(0)$, we performed $R(T)$ measurements under various external magnetic fields up to 8 T at other pressures (1.8, 31.2, 43.4, 95.5, and 155.9 GPa). We plotted T_c versus $\mu_0 H_{c2}(0)$ [fitted with the Ginzburg-Landan (GL) formula] at various pressures in Fig. 2(f). The results demonstrate that for pressures between 1.8 and 31.2 GPa, $\mu_0 H_{c2}(0)$ is initially insensitive to pressure. Then, it steadily decreases with pressure to 2.6 T at 155.9 GPa, indicating an inhibitory effect of high pressure.

We plotted the T_c of TaNbHfZr versus high pressure up to 157.2 GPa in Fig. 3(a). We can see a monotonically increasing T_c with pressure ranging from 1.1 to 45.8 GPa. After T_c reaches a broad maximum (around 15 K) within the pressure range of 45.8 to 79.8 GPa, then gradually decreases to 9.3 K at 157.2 GPa.

By ^{93}Nb-NMR spin-lattice relaxation rate measurement, a Hebel-Slichter coherence peak is seen just below T_c (shown in Supplement Material Fig. S4 [40]), indicating the s-wave pairing symmetry of the superconducting gap. Therefore, electron-phonon coupling is likely the primary factor for TaNbHfZr. Then, to explain the dome-shaped superconductivity in TaNbHfZr MEA, we performed

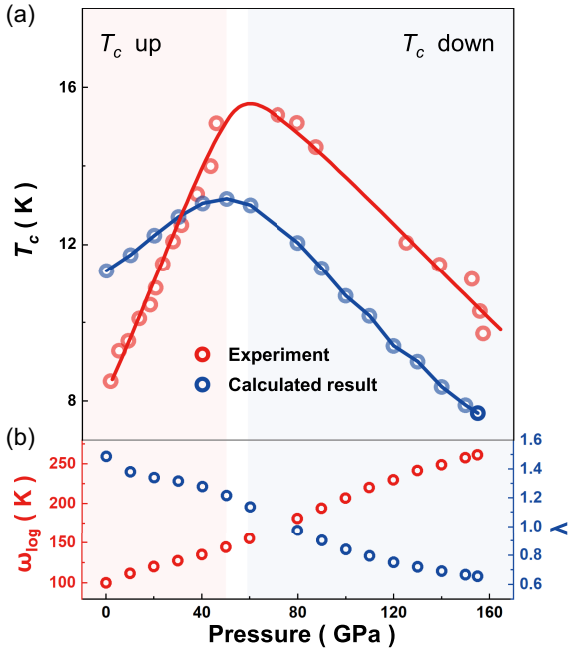

FIG. 3. (a) Pressure-dependent superconducting transition temperature of TaNbHfZr MEA (red) and the calculated evolution of superconducting transition temperature T_c (blue). (b) Logarithmically averaged characteristic phonon frequency $\omega_{\log}$ (red) and the electron-phonon coupling constant λ (blue) under high pressure.

first-principles calculations to explore the potential mechanism. The crystal structure is simulated via the virtual crystal approximation (VCA) method. The VCA is considered as an oversimplified method, but it is applicable when studying the high-entropy alloy, especially when the constituent elements are in adjacent rows or columns of the period periodic table [58,59]. To understand the pressure-dependent superconductivity detected experimentally, we calculated the superconducting transition temperature under different pressures by solving the Allen-Dynes-modified McMillan formula [60,61]. As indicated in Fig. 3(a), the calculated results show a dome-like superconducting diagram (T_{cmax} is 13.2 K at 50 GPa). This indicates the VCA simulation is acceptable for the TaNbHfZr system we studied. Above 50 GPa, the calculated T_c decreases at a faster rate than the observed T_c. This hysteresis behavior for the evolution of superconductivity with pressure may be caused by the disorder part in TaNbHfZr MEA [62]. According to the Allen-Dynes-modified McMillan formula, one can know that the superconducting transition temperature is related to the logarithmically averaged characteristic phonon frequency $\omega_{\log}$ and the electron-phonon coupling constant λ. We also plotted the evolution of $\omega_{\log}$ and λ in Fig. 3(b), one can see that the $\omega_{\log}$ is monotonically increasing and λ is monotonically decreasing with applying pressure. Figures 4(a)–4(c) show the phonon dispersion and the phonon density of states (phDOS) at 0, 50, and 155 GPa,

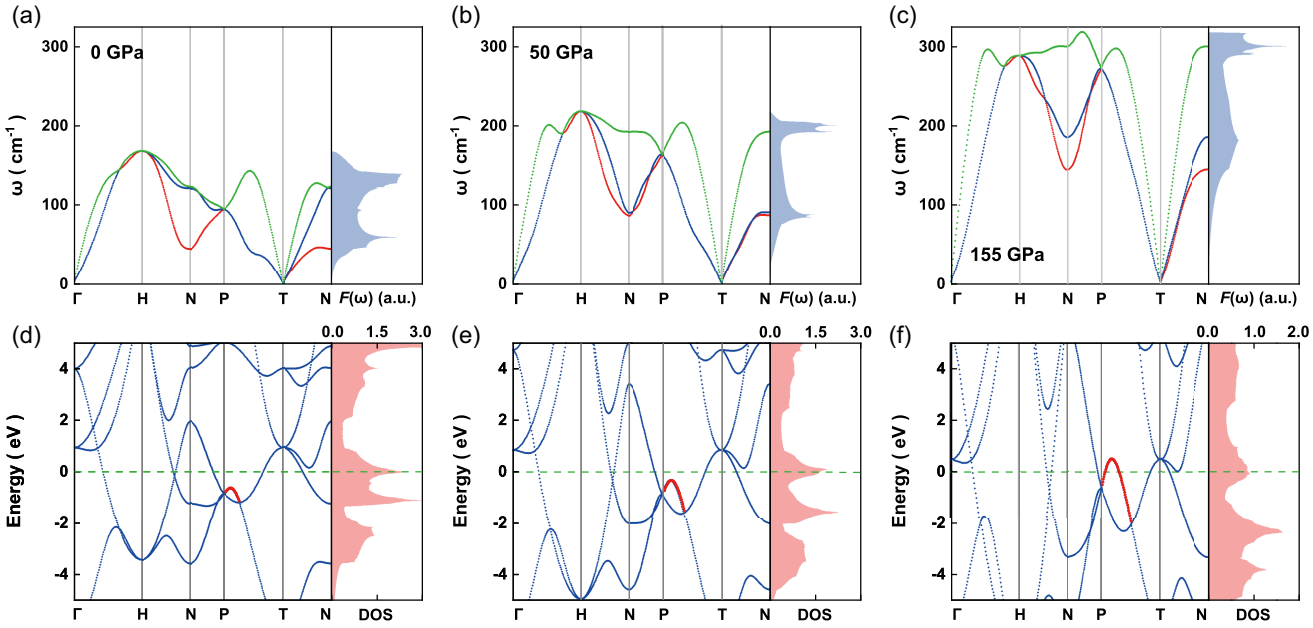

FIG. 4. (a)–(c) The phonon dispersion and phDOS at 0, 50, 155 GPa. (d)–(f) The band structure and DOS at 0, 50, 155 GPa.

one can see that the phonon frequency is increasing with increasing pressure, and the phDOS is broadened at the same time. Such pressure-induced blueshift of phonon frequency agrees well with the evolution of $\omega_{\log}$, and the larger $\omega_{\log}$ is conducive to superconductivity. It is worth noting that there are no imaginary frequencies in the phonon dispersion within the range of 0–155 GPa, indicating the stability of the bcc phase structure of TaNbHfZr MEA under high pressure (shown in Supplement Material Fig. S2 [40]).

When it comes to the band structures, we can see that the dispersion of the band around the Fermi level is enhanced with increasing pressure from Figs. 4(d)–4(f). Comparing the band structures at 0 and 50 GPa, there are band topological changes, indicating no Lifshitz transition under this pressure range. The calculated electron density of states (DOS) shows that the Fermi level is located at the shoulder of the density of states, but the maximum value of the shoulder is decreasing under high pressure. The decrease of the $N(E_F)$, λ leads to a reduction in the superconducting transition temperature based on the original BCS function [63,64], but the blueshift of $F(\omega)$ may cause a larger $\omega_{\log}$, which is beneficial to a higher superconducting transition temperature. So the dome-shaped curve may be attributed to the competing effects of the logarithmically averaged characteristic phonon frequency $\omega_{\log}$ and the electron-phonon coupling constant λ.

In summary, our study unveils the highest T_c (15.3 K at 71.6 GPa) in bcc—TaNbHfZr MEA with a dome-shaped superconductivity. The upper critical field at 0 K is 16.3 T deduced by fitting the GL equation. The zero-resistance state and upper critical fields are observed from ambient pressure to pressures as high as around 160 GPa, together with the high compressibility (The volume is compressed by about 21.5% at 50.5 GPa, and the third-order Birch-Murnaghan equation of state extrapolated change of the volume up to 157.2 from 50.5 GPa is about 37.5%, shown in the Supplemental Material Fig. S1d [40]). First-principles calculations attribute the dome-shaped curve to two competing effects, that is, the enhancement of the logarithmically averaged characteristic phonon frequency $\omega_{\log}$ and the simultaneous suppression of the electron-phonon coupling constant λ. The phonon dispersion at the range of 0–155 GPa proves the stability of the bcc phase under high pressure. The special dome-shaped superconductivity and the record-high T_c contribute to a better understanding of the differences and physical mechanisms of superconductivity between crystals and amorphous superconductors.

This work was supported by the National Key R&D Program of China (Grants No. 2021YFA1400300, No. 2021YFA0718700, No. 2023YFA1608901 and No. 2022YFA1403402), the National Natural Science Foundation of China (Grants No. 12374050, No. 12304095, No. 12375304, and No. 11974405), and the Strategic Priority Research Program of the Chinese Academy of Sciences (Grant No. CAS-WX2023SF-0101). The *in situ* XRD measurements were performed at 4W2 High Pressure Station, Beijing Synchrotron Radiation Facility (BSRF), which is supported by Chinese Academy of Sciences (Grants No. KJCX2-SW-N20 and No. KJCX2-SW-N03). Part of this work was partially carried out at the high-pressure synergetic measurement station of Synergic Extreme Condition User Facility.

X. H. Y. and F. H. conceived the project. L. W. loaded the sample for electrical transport measurement and x-ray diffraction; H. Z. collected the transport data; L. W., J. D., J. L., J. Y., and R. Z. performed NMR measurements; J. S. did the first-principles calculations under the supervision of M. L.; S. G. provided the sample; L. W. prepared the original manuscript; and all authors made comments.

*These authors contributed equally to this letter.
†Corresponding author: mliu@iphy.ac.cn
‡Corresponding author: hongfang@iphy.ac.cn
§Corresponding author: yuxh@iphy.ac.cn

[1] J. Chang, E. Blackburn, A. T. Holmes, N. B. Christensen, J. Larsen, J. Mesot, R. Liang, D. A. Bonn, W. N. Hardy, A. Watenphul *et al.*, Nat. Phys. **8**, 871 (2012).
[2] E. Morosan, H. W. Zandbergen, B. S. Dennis, J. W. G. Bos, Y. Onose, T. Klimczuk, A. P. Ramirez, N. P. Ong, and R. J. Cava, Nat. Phys. **2**, 544 (2006).
[3] J. Dong, H. J. Zhang, G. Xu, Z. Li, G. Li, W. Z. Hu, D. Wu, G. F. Chen, X. Dai, J. L. Luo *et al.*, Europhys. Lett. **83**, 27006 (2008).
[4] Z. A. Ren, G. C. Che, X. L. Dong, J. Yang, W. Lu, W. Yi, X. L. Shen, Z. C. Li, L. L. Sun, F. Zhou *et al.*, Europhys. Lett. **83**, 17002 (2008).
[5] D. F. Agterberg and H. Tsunetsugu, Nat. Phys. **4**, 639 (2008).
[6] K. Y. Chen, N. N. Wang, Q. W. Yin, Y. H. Gu, K. Jiang, Z. J. Tu, C. S. Gong, Y. Uwatoko, J. P. Sun, H. C. Lei *et al.*, Phys. Rev. Lett. **126**, 247001 (2021).
[7] F. H. Yu, D. H. Ma, W. Z. Zhuo, S. Q. Liu, X. K. Wen, B. Lei, J. J. Ying, and X. H. Chen, Nat. Commun. **12**, 3645 (2021).
[8] J. P. Rueff, S. Raymond, M. Taguchi, M. Sikora, J. P. Itié, F. Baudelet, D. Braithwaite, G. Knebel, and D. Jaccard, Phys. Rev. Lett. **106**, 186405 (2011).
[9] Q. Q. Liu, H. Yang, X. M. Qin, Y. Yu, L. X. Yang, F. Y. Li, R. C. Yu, C. Q. Jin, and S. Uchida, Phys. Rev. B **74**, 100506(R) (2006).
[10] W. E. Pickett, Rev. Mod. Phys. **61**, 433 (1989).
[11] T. Shibauchi, A. Carrington, and Y. Matsuda, Annu. Rev. Condens. Matter Phys. **5**, 113 (2014).
[12] G. E. D. K. Prawiroatmodjo, F. Trier, D. V. Christensen, Y. Chen, N. Pryds, and T. S. Jespersen, Phys. Rev. B **93**, 184504 (2016).
[13] K. Y. Tsai, M. H. Tsai, and J. W. Yeh, Acta Mater. **61**, 4887 (2013).
[14] B. Gludovatz, A. Hohenwarter, D. Catoor, E. H. Chang, E. P. George, and R. O. Ritchie, Science **345**, 1153 (2014).
[15] F. Otto, N. L. Hanold, and E. P. George, Intermetallics **54**, 39 (2014).
[16] S. Haas, M. Mosbacher, O. N. Senkov, M. Feuerbacher, J. Freudenberger, S. Gezgin, R. Völkl, and U. Glatzel, Entropy **20**, 654 (2018).
[17] O. N. Senkov, J. M. Scott, S. V. Senkova, D. B. Miracle, and C. F. Woodward, J. Alloys Compd. **509**, 6043 (2011).
[18] J. P. Couzinié, L. Lilensten, Y. Champion, G. Dirras, L. Perrière, and I. Guillot, Mater. Sci. Eng. A **645**, 255 (2015).
[19] A. Takeuchi, K. Amiya, T. Wada, K. Yubuta, and W. Zhang, J. Miner. Met. Mater. Soc. **66**, 1984 (2014).
[20] R. Soler, A. Evirgen, M. Yao, C. Kirchlechner, F. Stein, M. Feuerbacher, D. Raabe, and G. Dehm, Acta Mater. **156**, 86 (2018).
[21] J. W. Qiao, M. L. Bao, Y. J. Zhao, H. J. Yang, Y. C. Wu, Y. Zhang, J. A. Hawk, and M. C. Gao, J. Appl. Phys. **124**, 195101 (2018).
[22] L. Lilensten, J. P. Couzinié, L. Perrière, J. Bourgon, N. Emery, and I. Guillot, Mater. Lett. **132**, 123 (2014).
[23] S. Ranganathan, Curr. Sci. **85**, 1404 (2003).
[24] L. Sun and R. J. Cava, Phys. Rev. Mater. **3**, 090301 (2019).
[25] J. W. Yeh, J. Miner. Met. Mater. Soc. **65**, 1759 (2013).
[26] F. Otto, Y. Yang, H. Bei, and E. P. George, Acta Mater. **61**, 2628 (2013).
[27] P. Koželj, S. Vrtnik, A. Jelen, S. Jazbec, Z. Jagličić, S. Maiti, M. Feuerbacher, W. Steurer, and J. Dolinšek, Phys. Rev. Lett. **113**, 107001 (2014).
[28] X. Zhang, N. Winter, C. Witteveen, T. Moehl, Y. Xiao, F. Krogh, A. Schilling, and F. O. von Rohr, Phys. Rev. Res. **2**, 013375 (2020).
[29] S. G. Jung, Y. Han, J. H. Kim, R. Hidayati, J. S. Rhyee, J. M. Lee, W. N. Kang, W. S. Choi, H. R. Jeon, J. Suk *et al.*, Nat. Commun. **13**, 3373 (2022).
[30] C. heng, X. Zhang, M. J. R. Haché, and Y. Zou, Nano Res. **15**, 4873 (2022).
[31] K. Jasiewicz, B. Wiendlocha, P. Korbeń, S. Kaprzyk, and J. Tobola, Phys. Status Solidi RRL **10**, 415 (2016).
[32] Y. Yuan, Y. Wu, H. Luo, Z. Wang, X. Liang, Z. Yang, H. Wang, X. Liu, and Z. Lu, Front. Mater. **5**, 72 (2018).
[33] F. von Rohr, M. J. Winiarski, J. Tao, T. Klimczuk, and R. J. Cava, Proc. Natl. Acad. Sci. U.S.A. **113**, E7144 (2016).
[34] F. O. von Rohr and R. J. Cava, Phys. Rev. Mater. **2**, 034801 (2018).
[35] K. Stolze, F. A. Cevallos, T. Kong, and R. J. Cava, J. Mater. Chem. C **6**, 10441 (2018).
[36] K. Stolze, J. Tao, F. O. von Rohr, T. Kong, and R. J. Cava, Chem. Mater. **30**, 906 (2018).
[37] S. Marik, K. Motla, M. Varghese, K. P. Sajilesh, D. Singh, Y. Breard, P. Boullay, and R. P. Singh, Phys. Rev. Mater. **3**, 060602(R) (2019).
[38] J. Guo, H. Wang, F. von Rohr, Z. Wang, S. Cai, Y. Zhou, K. Yang, A. Li, S. Jiang, Q. Wu *et al.*, Proc. Natl. Acad. Sci. U.S.A. **114**, 13144 (2017).
[39] K. Y. Wu, S. K. Chen, J. M. Wu *et al.*, Nat. Sci. **10**, 110 (2018).
[40] See Supplemental Material at http://link.aps.org/supplemental/10.1103/PhysRevLett.132.166002, which includes Refs. [39,41–55] for details on our material (Sec. A), high-pressure synchrotron x-ray diffraction (Sec. B), high-pressure resistance measurements (Sec. C), nuclear magnetic resonance (Sec. D), and first-principles calculations (Sec. E).
[41] H. K. Mao, J. Xu, and P. M. Bell, J. Geophys. Res. **91**, 4673 (1986).
[42] C. Prescher and V. B. Prakapenka, High Press. Res. **35**, 223 (2015).
[43] G. K. Williamson and W. H. Hall, Acta Metall. **1**, 22 (1953).
[44] F. Birch, J. Geophys. Res. **83**, 1257 (1978).

[45] A. S. Ahmad, Y. Su, S. Liu, K. Ståhl, Y. Wu, X. Hui, U. Ruett, O. Gutowski, K. Glazyrin, H. P. Liermann *et al.*, J. Appl. Phys. **121**, 235901 (2017).
[46] M. I. Eremets, J. Raman Spectrosc. **34**, 515 (2003).
[47] J. Luo, C. Wang, Z. Wang, Q. Guo, J. Yang, R. Zhou, K. Matano, T. Oguchi, Z. Ren, G. Cao *et al.*, Chin. Phys. B **29**, 067402 (2020).
[48] J. Yang, Z. T. Tang, G. H. Cao, and G. Q. Zheng, Phys. Rev. Lett. **115**, 147002 (2015).
[49] J. Luo, J. Yang, R. Zhou, Q. G. Mu, T. Liu, Z. A. Ren, C. J. Yi, Y. G. Shi, and G. Q. Zheng, Phys. Rev. Lett. **123**, 047001 (2019).
[50] P. Giannozzi, S. Baroni, N. Bonini, M. Calandra, R. Car, C. Cavazzoni, D. Ceresoli, G. L. Chiarotti, M. Cococcioni, I. Dabo *et al.*, J. Phys. Condens. Matter **21**, 395502 (2009).
[51] L. Bellaiche and D. Vanderbilt, Phys. Rev. B **61**, 7877 (2000).
[52] J. P. Perdew and A. Zunger, Phys. Rev. B **23**, 5048 (1981).
[53] S. Baroni, S. de Gironcoli, A. Dal Corso, and P. Giannozzi, Rev. Mod. Phys. **73**, 515 (2001).
[54] P. B. Allen and R. C. Dynes, Phys. Rev. B **12**, 905 (1975).
[55] R. C. Dynes, Solid State Commun. **10**, 615 (1972).
[56] C. Armstrong, P. Rae, D. Tasker, E. Heatwole, and B. Broilo, AIP Conf. Proc. **1979**, 160001 (2018).
[57] Z. Duan, Y. Liu, A. Pi, and F. Huang, Meas. Sci. Technol. **22**, 075206 (2011).
[58] Z. Huang, Z. Li, D. Wang, Y. Shi, M. Yan, and Y. Fu, J. Phys. Chem. Solids **151**, 109859 (2021).
[59] F. Tian, Front. Mater. **4**, 36 (2017).
[60] W. L. McMillan, Phys. Rev. **167**, 331 (1968).
[61] P. B. Allen and R. C. Dynes, Phys. Rev. B **12**, 905 (1975).
[62] J. F. Zhang, M. Gao, K. Liu, and Z. Y. Lu, Phys. Rev. B **102**, 195140 (2020).
[63] J. Bardeen, L. N. Cooper, and J. R. Schrieffer, Phys. Rev. **108**, 1175 (1957).
[64] J. Bardeen, L. N. Cooper, and J. R. Schrieffer, Phys. Rev. **106**, 162 (1957).